SCIENTIFIC PROGRESS REPORT - PROJECT PN-III-P1-1.1-PD-2016-0172,

EXPLORING PERMAFROST OCCURRENCE AND EVOLUTION IN THE RILA AND PIRIN MOUNTAINS (BULGARIA) USING A COMBINED GEOMRPHOLOGICAL, GEOPHYSICAL AND DENDROCHRONOLOGICAL APPROACH

REPORT 2 (01.01.2019 – 31.12.2019)

REPORT 2: Exploring permafrost occurrence in the test sites (second part), assessing the ground surface temperature of rock glaciers and the dynamics of the rock glaciers (second part)

Abstract

In this phase we continued the thermal (bottom temperature of the snow cover - BTS, ground surface temperature monitoring - GST and spring water termperature), geophysical and topographical measurements started in the previous year. In addition, we enriched the database containing temperature data and horizontal displacements of selected blocks within rock glaciers. A statistical approach was also applied to examine the linkages between thermal regime and local topo-climatic factors. Tree-ring analysis of *Pinus Mugo* installed on two different rock glaciers was also performed within this phase.

Scientific description

In this phase we have planned nine different activities, as follows:

1. BTS measurements and spatial analysis of achieved values.
2. Geophysical measurements and processing geophysical data.
3. Processing all the thermal data achieved.
4. Calculating specific thermal indices (mean annual grouns surface temperature – MAGST; winter equilibrium temperature – WeqT, GST evolution, freezing and thaving indices and `zero curtain` period).
5. Assessing the cooling effect of the coarse deposits (e.g., thermal convection, chimney effect, low thermal conductivity).
6. Statistical analysis of the relationships between GST and local topo-climatic factors.
7. Assessing the dynamics of rock glaciers by ground-based topographic measurements.
8. Tree-ring analysis of Pinus Mugo growing on rock glaciers.
9. UAV photogrammetry and Structure from Motion for high resolution digital elevation model production and monitoring long term horizontal displacement of blocks.

1. BTS measurements and spatial analysis of achieved values

The BTS method is one of the most efficient for permafrost mapping and has been widely used in different alpine environments. Classical BTS measurements using two lightweight BTS probes equipped with digital thermometers were carried out at the end of 2018-2019 winter season. Two long probes (2.5 m in length) equipped with digital thermometers (0.1ºC precision) were used to

measure the temperature at the bottom of the snow cover. According to „rules of thumb" values lower than -3°C indicate that permafrost occurrence is probable, values of -2 to -3°C suggest the possible presence of permafrost while values higher than -2°C indicate the absence of permafrost (Hoelzle et al., 1999).

We planned our BTS investigations on four different rock glaciers (M3 and M4 in Rila Mountains and P8 and P9 in Pirin Mountains). We made similar investigations at these sites in the previous two years. The BTS points were collected in March 2019, when the ground was covered by a thick snow cover (fig. 1)

Fig. 1. BTS investigations in March 2019.

In total we collected 83 BTS points (table 1).

Table 1. Characteristics of BTS values measured in March 2019.

Site code	No. of measurements	Mean BTS (°C)	Minimum BTS (°C)	Maximum BTS (°C)	Mean thickness of snow (cm)
M4	31	-3.4	-5.4	-1.5	142
M3	21	-2	-5.5	0.3	128
P9	21	-4.1	-5.7	-1.9	172
P8	10	-2.5	-3.6	-2.4	162

At site M4 we measured 31 points, from which 28 were made within the outline of the rock glacier, two on a protalus rampart and one outside the rock glacier (fig. 2). Only one BTS value indicated the absence of permafrost, whereas 10 BTS values suggested the possible presence of permafrost and 19 the probable occurrence of permafrost at this site. The mean BTS value for this rock glacier was -3.4°C and it was lower than the corresponding value measured in the previous two years (Onaca et al., in press).

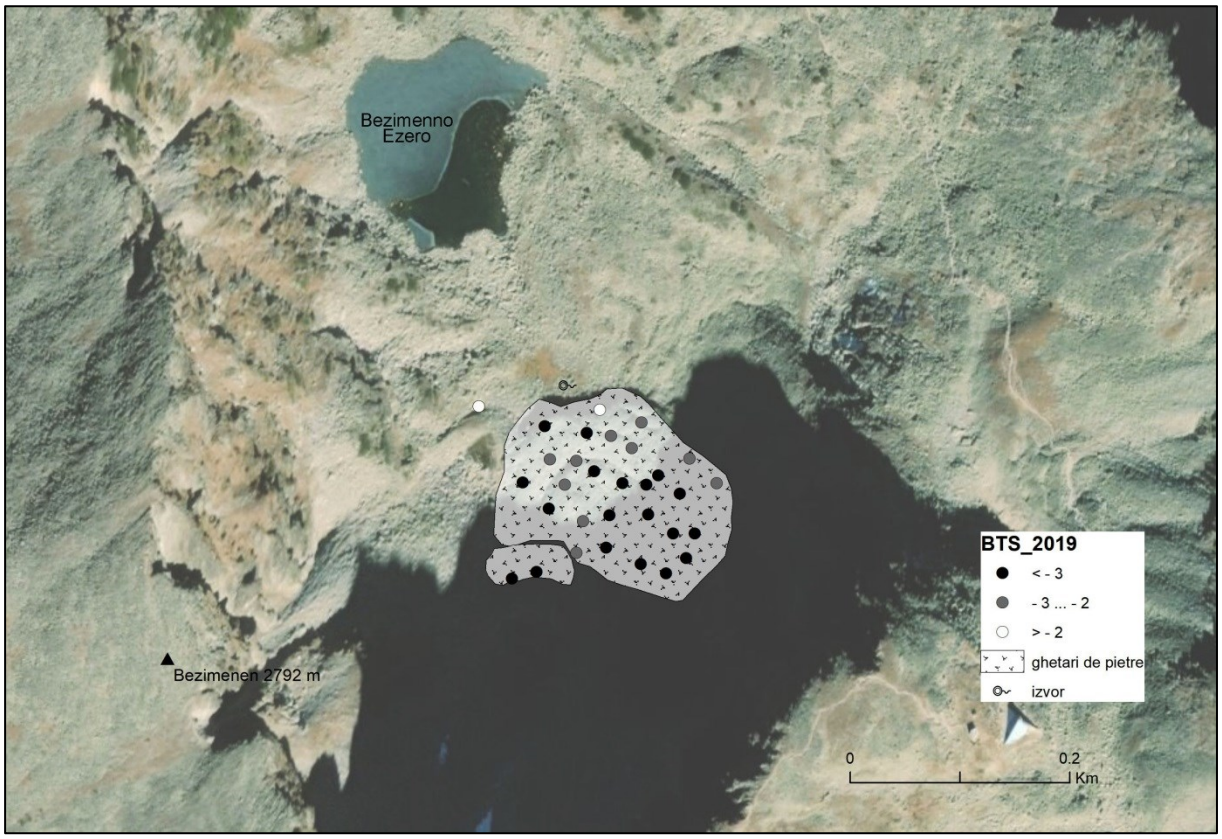

Fig. 2. BTS value measured on M4 rock glacier.

In case of M3 rock glacier, only five BTS values indicated the probable presence of permafrost, but three of these were located on a debris cone feeding the rock glacier. Within the rock glacier outline, four BTS values indicated the absence of permafrost, four suggested the possible presence and two the likely occurrence. The mean BTS value for this rock glacier was -2.2°C, with 1,2°C lower than in March 2018 (Onaca et al., in press).

In the Pirin Mountains, from 31 BTS points, two were measured outside the rock glaciers outlines for comparisons. Both values were greater than -2°C, confirming the absence of permafrost at those locations.

In case of P9, 18 BTS values were lower than -3°C confirming that like in previous years the permafrost is probable to occur at this site. Only two values were between -2°C and -3°C suggesting the possible presence of permafrost, whereas near the front of the rock glacier one BTS point has a -1.9°C value. At P8 site only at three locations the BTS point indicated the probable presence of permafrost, whereas in five location the permafrost is possible. The lowest BTS value recorded was on the P9 rock glacier (-5.7°C). At this site was also calculated the lowest mean BTS (-4.1°C), with 0.6°C lower than in the 2016-2017 cold season (Onaca et al., in press).

The thickness of snow cover was above 100 cm at all the locations where we made BTS measurements. In the Pirin Mountains the snow cover thickness was greater than in Rila Mountains. In M4 site the snow cover had a similar thickness with the one measured in 2017, but greater than in 2018. In the Pirin Mountains the snow cover was greater than in 2017, but thinner than in 2018. At M3 we observed also several funnels in the snow.

2. Geophysical measurements and processing geophysical data (second part)

In this phase we have continued to investigate the internal structure of rock glaciers using geophysical methods. Two different campaigns were organized, one during the time of BTS measurements (March) and one in September (fig. 3). We used a MALA ProEx GPR equiped with unshielded *Rough Terrain* antensas of 50 and100 Mhz. This method is suitable to investigate low electrical conductivity materials (e.g. ice, sand, bedrock etc.).

Fig. 3. GPR investigations performed in September (a) and March (b) 2019.

As Common Midpoint (CMP) or Wide Angle Reflection and Refraction (WARR) measurements are impossible using RTA antennas an overall wave velocity of 0.15 m/ns was used for the depth conversion of the radar signal (Onaca et al., 2015). GPR data processing and interpretation was performed using Reflexw 4.5, applying a sequence exemplified in similar studies (Ardelean et al., 2017). Background noise was eliminated by applying a *running average* filter, whereas for signal saturation a *dewow* filter was used. In order to compensate for the attenuation factor of radar signal with depth *energy decay* filter was applied. The last stages of processing included the application of *zero time corrections*, *background removal* and *bandpassfrequency*, as well as *topographic correction* to render the local topography of the investigated rock glaciers

We performed 26 GPR profiles with lengths between 70 and 330 m. The maximum depth of penetration was between 16 and 34 m. We identified three types of situations, regarding the occurrence of permafrost:

1. The presence of permafrost was identified on the entire length of the profile or at least on a considerable part of the radargram. This situation was identified in case of M4, P9, B14 and K2 rock glaciers. In these cases we were able to identify four types of reflections, which were interpreted as (1) the base of the snow cover; (2) the base of the active layer; (3) the floor of the rock glaciers; (4) stacked reflections. Our findings showed that the active layer was very thick (between 4 and 12 meters). Within this layer there are many reflections, suggesting the presence of a coarse layer with voids and/or seasonal ice lenses (Otto et al., 2012). Below the active layer we identified another layer characterized by high amplitudes of the electromagnetic waves and 7 to 14 meters thick which was interpreted as permanently frozen (Angelopoulos et al., 2013). The bedrock was intercepted between 15 and 33 m.
2. The presence of permafrost is patchy along the profile line and it seems that permanently frozen ground occurs only in specific areas, such as: G1, P10, P7, P8, P10, B11, B12, B15. In these cases the thickness of the active layer is great as well (between 6 and 13 m). The main characteristic

of this typology is that permafrost occurs only on small areas. The thickness of most of these rock glaciers is around 15 m.

3. The presence of permafrost was not detected. It is the case of K1, M3, G2, P5, P6 and B13 rock glaciers. In these situations we were unable to identify any sharp reflection characterized by high velocities of the electromangnetic waves, specific for permafrost. The mean thickness of these rock glaciers is between 13 and 22 m.

3. Processing all the thermal data achieved

Within this project we performed three types of thermal measurements: i) BTS measurements at the end of the cold season; ii) continuous GST monitoring and iii) spring water temperature at the end of warm season.

In case of BTS values the processing consisted in calculating the mean/minimum/maximum values of BTS for each rock glacier, the mean thickness of snow as wel as the number of points indicating probable/possible or improbable occurrence of permafrost. All these calculations were done in Microsoft Excel and after that transferred in ArcGIS where the maps with the distribution of BTS values were realized.

For the monitoring of the GST we used iButtons DS1922L thermistors installed in 2018 and 2016. In September 2019 we downloaded all the recorded data in a portable computer. Initially the data were in .txt format, but we changed it to .xls. The processing process consisted in the evaluation of all the values and making necessary corrections (e.g., deleting the values recorded before setting the thermistors in the field; adjusting the values using the `zero curtain` interval values). After all these corrections we calculated several specific indices (ex: mean annual ground surface temperature – MAGST; winter equilibrium temperature – WeqT, freezing and thawing indices and the date of snow dissapearence).

In September 2019 we also measured the temperature of several springs seeping from the base of the rock glaciers using a handheld thermometer with ± 0.5°C accuracy. For each measurement location we recorded information about the geographical coordinates, measurement date, site code and air temperature. The values recorded in September 2019 were: K1 – 2,2°C; K2 – 3,2°C; P6 – 6,3°C; B12 – 6,5°C; B14 – 0,9°C; B15 – 2,4°C.

4. Calculating specific thermal indices (mean annual grouns surface temperature – MAGST; winter equilibrium temperature – WeqT, GST evolution, freezing and thaving indices and `zero curtain` period)

Table 2 reveals the results of the thermal indices extracted from the GST values recorded at K1 and K2 site. Permafrost is probable to occur at all the location in K2, but only in one location in K1 is possible. The MAGST values are very low in all the cases, whereas the mean freezing index is considerably lower at K2 compared with K1. At K1.1 the snow disappeared completely in 13 August, resulting in a prolonged zero curtain interval. At all the sites in K2 the MAGST values are negative and the freezing index is below -800°C days.

In site B we monitored GST values of two rock glaciers, one talus cone, one protalus rampart and two rock walls. Excepting the rock walls, in most of the sites the MAGST was negative. WeqT ssuggested probable permafrost conditions in M4, whereas in M3 only one location showed possible

permafrost conditions. Permafrost presence in the investigated rock walls is unlikely, but is probable to occur in the talus cone and protalus rampart.

Table 2. Thermal indices at site A.

Code site	Code location	Morphology	MAGST	WeqT	GFi	GTi	0 curtain
A	**K1.1**	GP	0.0	0	-192.63	189.38	161
	K1.2	GP	0.7	-0.8	-324.71	782.19	76
	K1.3	GP	0.5	-1.7	-363.80	742.19	64
	K1.4	GP	0.2	-2.1	-474.53	686.16	58
	K2.1	GP	-0.3	-3.6	-864.56	730.36	23
	K2.2	GP	-0.8	-4	-1004.68	713	33
	K2.3	GP	-0.6	-3.7	-894.32	694.14	36
	K2.4	GP	-0.2	-3.2	-821.45	786.25	44

GP – rock glacier.

Table 3. Thermal indices at site B.

Code site	Code location	Morphology	MAGST	WeqT	GFi	GTi	0 curtain
B	**M3.1**	GP	-1.36	-	-1047.30	550.47	47
	M3.2	GP	-0.37	-	-682.15	546.82	50
	M3.3	GP	-0.12	-2.12	-632.81	568.45	39
	M3.4	GP	0.41	-1.45	-581.93	670.13	42
	M4.1	GP	-2.19	-4.97	-1102.43	302.34	55
	M4.2	GP	-1.85	-4.06	-793.88	117.97	68
	M4.3	GP	-1.12	-3.21	-577.98	169.77	86
	M4.4	GP	-0.54	-3.68	-761.10	570.3	36
	M4.5	GP	-1.41	-4.13	-779.03	265.19	48
	M4.6	GP	-0.73	-3.86	-812.07	584.25	37
	M4.7	GP	-0.47	-3.25	-694.11	543.14	43
	M4.8	GP	-1.64	-3.53	-674.16	490.15	67
	M4.9	CG	0.18	-3.69	-786.11	852.51	25
	M4.10	PR	-1.83	-5.43	-1126.31	459.86	36
	M4.11	P	1.00	-	-785.32	1151.99	-
	M4.12	P	2.28	-	-816.48	1647.72	-

GP – rock glacier; PR – protalus rampart; CG – talus cone; P – rock wall.

The thermal measurements performed in site C are highlighted in table 4. Accoring to measurements permafrost is possible at G1.1 and G1.2 locations.

Table 4. Thermal indices at site C.

Code site	Code location	Morphology	MAGST	WeqT	GFi	GTi	0 curtain
C	**G1.1**	M	0.13	-2.30	-438.76	487.77	66
	G1.2	VG	-0.91	-2.27	-347.79	15.87	87
	G1.3	VG	0.42	-0.57	-491.23	502.58	72
	G1.4	VG	0.35	-1.54	-407.53	554.31	70
	G2.1	M	2.23	-0.24	-392.41	709.34	54
	G2.2	VG	-0.03	-0.34	-48.56	34.29	107
	G2.3	CG	0.56	-1.47	-457.35	603.25	63
	G2.4	PR	0.21	-1.89	-537.23	485.32	71

M – moraine; PR – protalus rampart; CG – talus cone; VG – scree slope.

In site D we analysed six rock glaciers, one talus cone, one protalus rampart, two rock walls, one block stream and one soliflcution lobe. In addition one thermistor measured air temperature variation (table 5). Accroding to the WeqT values permafrost is probable in P9 and P10 and may occur only in some locations in P5, P6, P7 and P8. During field work in September we noticed that snow was still present in some shaded places. MAGST values are also, very low, indicating that the thermal conditions are favorable for permafrost maintanence. Permafrost is unlikely to occur in rock walls, block stream or solifluction lobe, but is possible to occur in talus cone and protalus rampart.

Table 5. Thermal indices at site D.

Code site	Code location	Morphology	MAGST	WeqT	GFi	GTi	0 curtain
D	**P5.1**	GP	-0.42	-3.31	-737.07	583.1	79
	P5.2	GP	1.53	-1.74	-319.22	680.24	58
	P5.3	GP	0.91	-0.72	-359.14	753.12	52
	P5.4	GP	1.22	-2.02	-672.14	613.13	65
	P5.5	RP	3.11	-0.33	-98.03	1234.57	44
	P6.1	GP	0.83	-2.20	-463.13	765.58	53
	P6.2	GP	1.39	-1.36	-268.26	775.87	46
	P6.3	GP	1.14	-1.79	-398.12	691.32	57
	P6.4	GP	1.65	-1.12	-366.34	748.52	48
	P7.1	GP	1.87	-3.19	-533.11	1216.54	31
	P7.2	GP	1.08	-2.04	-475.26	870.95	41
	P7.3	GP	1.53	-1.97	-434.75	983.21	35
	P7.4	GP	2.08	-0.94	-254.14	1121.24	42
	P7.5	GP	1.91	-1.35	-309.13	863.15	46
	P7.6	GP	2.32	-0.83	-254.44	1015.24	48
	P7.7	CG	1.20	-2.38	-501.44	939.37	52
	P7.8	P	2.69	-	-579.96	1562.05	-
	P7.9	LS	2.58	-	-325.29	1267.29	26
	P8.1	GP	-0.20	-2.29	-455.93	382.17	56
	P8.2	GP	1.13	-1.63	-331.34	744.20	48
	P8.3	GP	0.85	-3.56	-504.02	815.13	58
	P8.4	GP	0.52	-2.74	-494.27	775.37	43
	P8.5	GP	0.02	-3.16	-524.11	694.20	55
	P8.6	GP	0.94	-2.23	-473.28	682.19	44
	P8.7	GP	1.32	-1.84	-486.21	734.76	47
	P8.8	GP	1.09	-1.74	-394.35	805.54	42
	P8.9	PR	0.82	-2.91	-471.51	771.11	50
	P9.1	GP	0.39	-3.63	-650.66	792.05	35
	P9.2	GP	0.15	-2.40	-460.36	519.94	54
	P9.3	GP	-1.06	-3.50	-609.75	221.96	73
	P9.4	GP	-1.18	-3.62	-564.40	132.28	100
	P9.5	GP	-0.54	-3.32	-522.38	323.88	58
	P9.6	GP	-0.42	-3.15	-603.17	448.61	67
	P9.7	GP	-1.24	-3.65	-709.23	257.89	93
	P9.8	GP	-1.11	-3.57	-680.06	274.25	76
	P10.1	GP	0.35	-3.51	-614.45	741.90	47
	P10.2	GP	0.36	-3.11	-576.91	707.36	55
	P10.3	GP	0.43	-2.97	-583.13	712.34	49
	P10.4	GP	0.52	-2.68	-577.43	744.30	46
	P10.5	P	1.52	-	-798.66	1353.2	-
	P10.6	A	-0.75		-1207.48	931.11	-

GP – gheţar de pietre; PR – protalus rampart; CG – con de grohotiș; P – perete; LS – lob de solifluxiune, RP – râu de pietre; A – aer.

In site E we analysed the GST of five rock glaciers (tabel 6). In B14 permafrost is probable at all the locations, the MAGST are negative and GFi values are also very high. Permafrost is also possible/probable in the other rock glaciers too.

Table 6. Thermal indices at site E.

Code site	Code location	Morphology	MAGST	WeqT	GFi	GTi	0 curtain
E	**B11.1**	GP	0.56	-2.23	-578.13	714.21	45
	B11.2	GP	0.82	-2.77	-537.44	721.09	48
	B11.3	GP	1.13	-	-471.21	809.41	41
	B11.4	GP	1.52	-1.43	-455.09	873.54	39
	B12.1	GP	0.37	-3.02	-682.74	817.69	53
	B12.2	GP	0.51	-2.96	-659.03	822.45	51
	B12.3	GP	0.63	-2.68	-612.77	851.23	53
	B12.4	GP	0.92	-2.28	-585.39	884.09	47
	B13.1	GP	0.53	-5.17	-869.78	1062.85	34
	B13.2	GP	0.91	-	-812.49	1124.51	31
	B13.3	GP	1.14	-2.52	-642.12	1037.81	41
	B13.4	GP	1.17	-2.30	-594.15	1147.15	37
	B14.1	GP	-1.85	-4.42	-889.95	213.81	74
	B14.2	GP	-1.52	-4.82	-983.88	430.59	36
	B14.3	GP	-0.81	-4.51	-737.71	440.81	60
	B14.4	GP	-1.52	-4.66	-1017.57	461.92	34
	B14.5	GP	-2.69	-6.79	-1273.43	289.93	67
	B14.6	GP	0.92	-4.83	-810.91	1145.03	33
	B14.7	GP	-0.47	-4.03	-814.33	509.22	59
	B14.8	GP	0.53	-3.87	-783.12	493.22	67
	B15.1	GP	-0.94	-4.87	-948.75	604.98	57
	B15.2	GP	-0.31	-3.95	-803.16	672.14	53
	B15.3	GP	0.76	-3.21	-709.12	804.22	45
	B15.4	GP	0.43	-2.87	-691.32	903.24	39
	B15.5	GP	-0.13	-4.51	-862.12	689.15	59
	B15.6	GP	0.91	-3.12	-781.21	813.41	46

GP – rock glacier;

Analyzing the thermal regime of GST during 2018-2019 season we identified four different types, according to the temperature characteristics during the winter.

a. GST evolution reveals below -3°C values in the `BTS window`. In autumn and early winter under thins snow cober the substrate is cooled intensively, as a result of air exchange with the atmosphere (fig. 4). After the onset of the insulating layer, the temperature values remain very low and constant. This type of regime is typical for sites with permafrost (Hoelzle et al., 1999). In our case this regime was observed in case of K2, M4, P7, P8, P9, P10, B12, B13, B14 and B15 rock glaciers.
b. GST values are between -2 and -3°C at the end of cold season below a thick insulating layer (fig. 5). This type of thermal regime is typical foar sites where the occurrence of permafrost is possible. In the se locations more investigations are required to elucidate if permafrost occur. In some of these locations in the previous seasons the values were below -3°C. This type of regime was observed at K1, M3, G1, P5, P6, P7, P8, P9, P10, B11, B12, B13 and B15 locations.

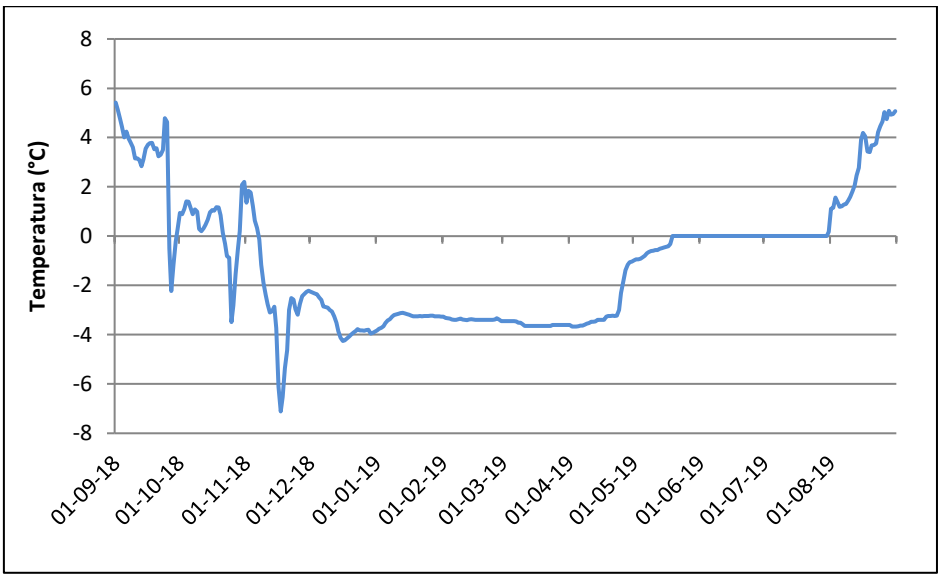

Fig. 4. Mean daily ground surface temperature at P9.3.

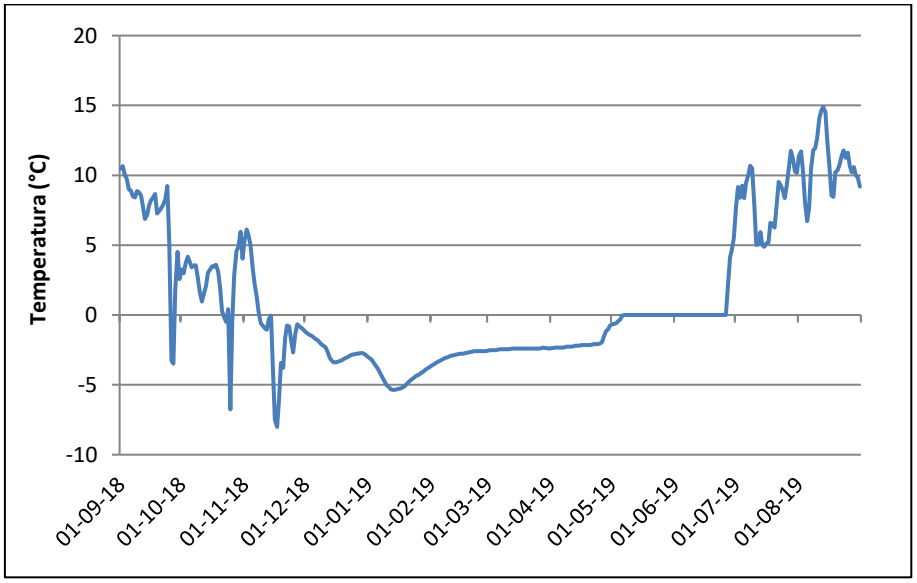

Fig. 5. Mean daily ground surface temperature at P9.2.

c. This regime is characterised by relatively high values of WeqT at the end of the winter (between 0 and -2°C). The temperature evolution is constant and does not show temperature fluctuations, indicating that permafrost in unlikely (fig. 6). This regime was observed at K1, M3, P5, P6, P7, P8 și B11, but also in G1 and G2.

d. The evolution of the temperature during the winter is characterized by significant temperature fluctuations. This regime coincides with the sites where during the winter the snow cover was either to thin, or there were funnels in the snow cover allowing air exchange with the atmosphere. At these sites permafrost occurrence should be investigated with other methods, too (Ishikawa, 2003). An example of this type of regime is illustrated in fig. 7. This type of regime is characteristics for M3, B11 and B13.

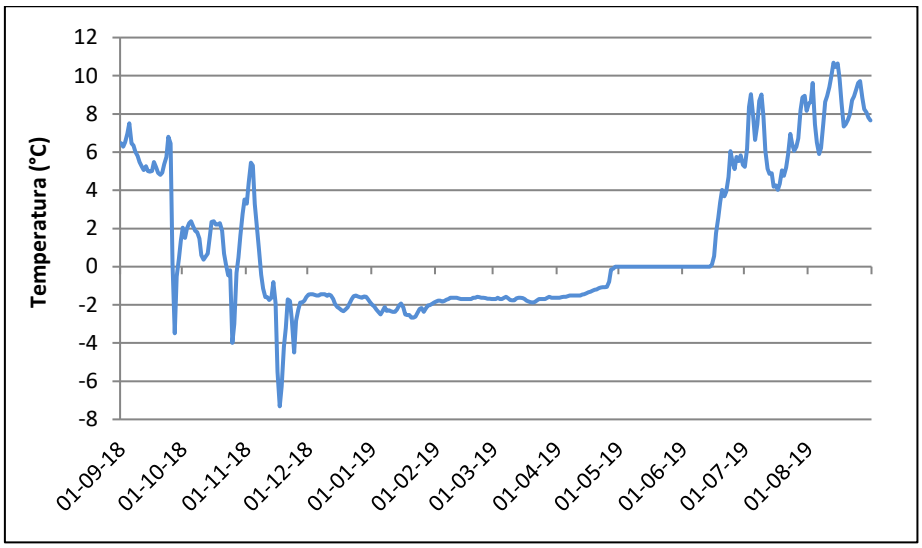

Fig. 6. Mean daily ground surface temperature at P8.2.

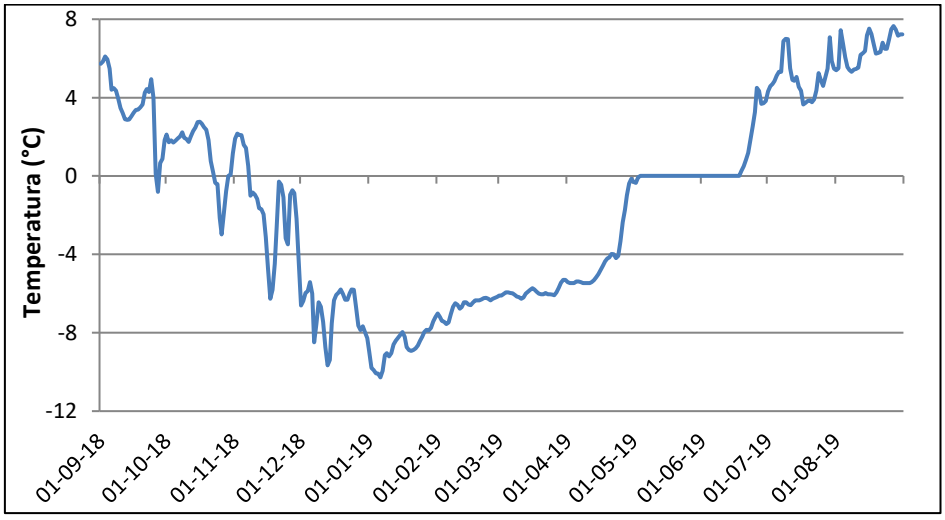

Fig. 7. Mean daily ground surface temperature at M3.1.

5. Assessing the cooling effect of the coarse deposits (e.g., thermal convection, chimney effect, low thermal conductivity).

Snow cover plays a decisive role on GST regime small-scale variability. After the onset of the insulating snow cover isothermal conditions characterize the surface of the ground. In several cases (G1.2 or G2.2) the ground was covered by snow for more than 350 days in the 2018-2019 season. At these sites the maximum temperatures recorded at the end of August 2019 was below 5°C.

Between October and December, until the onset of the insulating snow cover, the continuous air exchange with the atmosphere favored the cooling of the active layer. This mechanism was extremely efficient during cold episodes, when because of free convection cold air replace warm air within the coarse deposits. Now, the minimum values of temperatures are recorded at all the sites (between -5 and -15°C) (fig. 8).

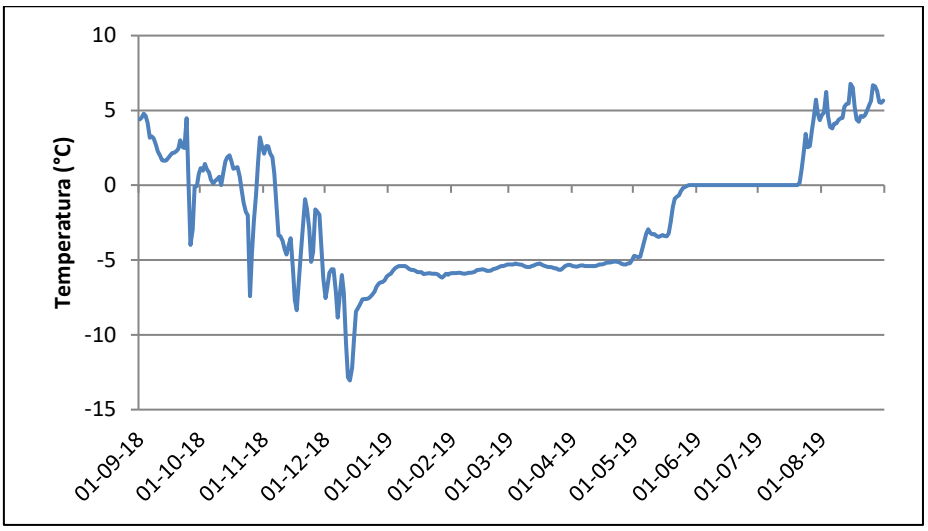

Fig. 8. Mean daily ground surface temperature at M4.1.

In some cases, at the beginning of winter and during the cold seasons, chimney mechanisms operated at different sites (fig. 9). As a result of the air advection warm air was expelled at the upper part of some rock glaciers. In most of the cases the temperature at the surface of of the coarse deposits are mainly controlled by conductive mechanisms (Gruber, Hoelzle, 2008) (fig. 10). This additional mechanism for cooling the ground operates exclusively during the winter, when a sufficiently thick snow covers the ground. In coarse deposits, with high porosity, this mechanism is able to decrease the thermal conductivity of the ground. Because of this mechanism the warming of the ground which normally occur below the snow cover is absent, resulting instead the cooling of the debris surface.

This mechanism is strongly controlled by snow cover, but slope or surface exposure plays an important role too.

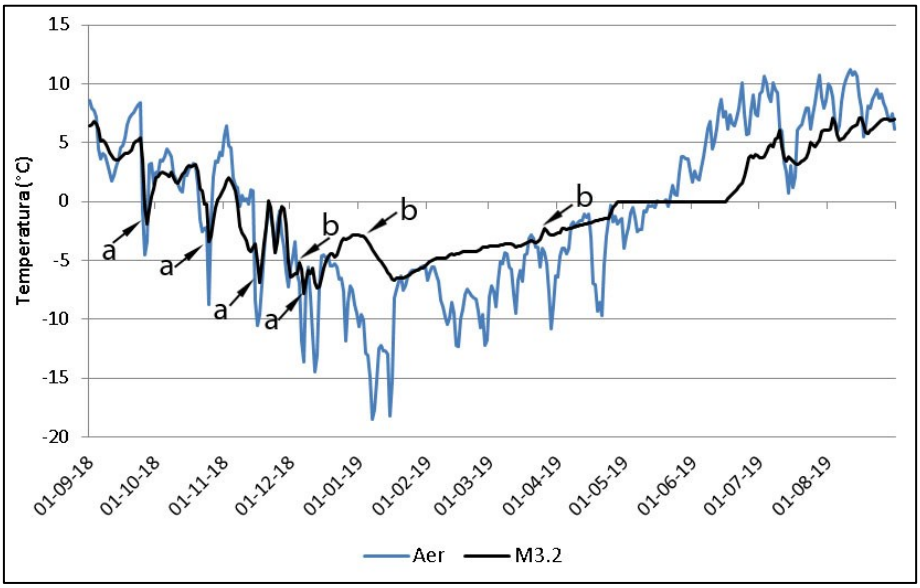

Fig. 9. Mean daily air and ground surface temperature. Arrows indicate intense cooling of the ground by efficient winter convection (a), inverse behavior due to air ventilation (b).

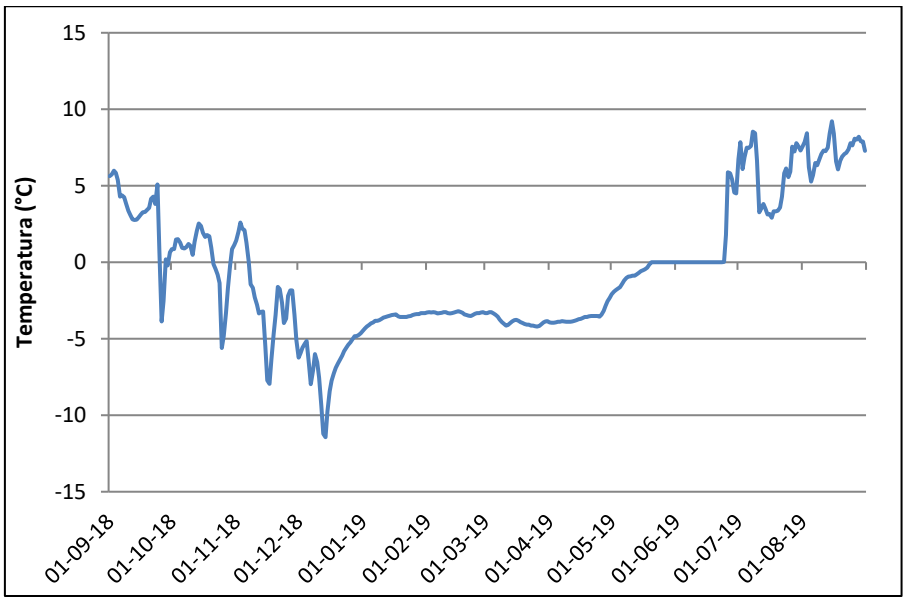

Fig. 10. Mean daily ground surface temperature at M4.4.

6. Statistical analysis of the relationships between GST and local topo-climatic factors.

Air temperature has the greatest influence on the GST regime. At most of the sites there is a strong dependence between air temperature and GST value (the correlation factor is above 0.6). The lowest influence of air temperature correspond with the locations where snow persisted until August and where the correlation factor is below 0,6.

The results of linear regressions revealed weak dependencies of GST with slope, curvature or solar radiation. The strongest statistical relationships are with snow cover and elevation, but are considerable weaker then the correlation with air temperature.

Table 7. Results of linear regression between GST and local topo-climatic factors.

Elevation vs	**r**	**p-value**	**Slope vs**	**r**	**p-value**	**Cuvature vs**	**r**	**p-value**
WeqT	**0.09***	0.010	WeqT	0.00	0.944	WeqT	0.01	0.336
MAGST	**0.14***	0.000	MAGST	0.00	0.877	MAGST	0.00	0.666
GFi	0.03	0.081	GFi	0.00	0.588	GFi	0.00	0.708
GTi	0.09	0.004	GTi	0.00	0.966	GTi	0.00	0.851
0 curtain	0.00	0.560	0 curtain	0.00	0.797	0 curtain	0.00	0.954
Potential radiation vs	**r**	**p-value**	**Snow cover duration vs**	**r**	**p-value**			
WeqT	0.02	0.153	WeqT	0.00	0.466			
MAGST	0.00	0.644	MAGST	**0.47***	0.000			
GFi	0.00	0.374	GFi	0.01	0.310			
GTi	0.03	0.073	GTi	**0.54***	0.000			
0 curtain	0.02	0.193	0 curtain	**0.56***	0.000			

r – Correlation coefficent; p-value – Pearson value; * significant correlation (significance level p=0.01).

7. Assessing the dynamics of rock glaciers by ground-based topographic measurements.

Measurements of movement of five rock glaciers in the Rila and Pirin Mountains were initiated in 2018 using high precision DGPS system from Topcon. In August-September 2019 we measured the first annual horizontal rates of displacements for several points marked in 2018. The magnitude of the horizontal movement, as well as the direction of movement was determined for P8, P9, P10 and M3 and M4. On each rock glacier we monitored between 10 and 28 blocks.

Despite the high accuracy of the GPS systems we estimated that only the values representing movement greater than 2 cm can be attributed to rock glacier movement, whereas values smaller than 2 cm might be in the range of the errors.

At M3 rock glacier we measured 15 points, and as we expected all the measured values are below 2 cm/year. It is likely that this rock glacier is iactive/relict, considering that is covered by vegetation on a high degree.

At M4 only four points from a total of 18 revealed horizontal movement below 2 cm/year. 77% of the total points showed horizontal movement higher than 2 cm/year, indicating that probably this rock glacier is an active one. The highest number of monitored blocks recorded a velocity between 2 and 5 cm/year, whereas two points showed movement rates between 5 and 10 cm/year. Other two points revealed movement rates higher than 10 cm/year (in one case we measured 29 cm/year in the southern part of the rock glacier).

At P8 from 15 blocks only eight revealed horizontal movement between 2 and 5 cm/year, whereas one point showed a horizontal movement between 5 and 10 cm/year. At P9 only in five situations the movements was below 2 cm/year, in 18 cases the horizontal velocity of the blocks was between 2 and 5 cm/year and in foru cases between 5 and 10 cm/year. P10 was the smallest rock glacier we investigated. On his surface we monitored 11 points and only six of these moved with more than 2 cm, but less than 5 cm between the summer of 2018 and 2019.

8. Tree-ring analysis of Pinus Mugo growing on rock glaciers.

In this study we sampled 30 shrubs of Pinus Mugo located on two different rock glaciers (one is below Lovnitsa peak in Rila Mountains and the other is near Popovo Lake in Pirin Mountains). The sampling was performed in September 2019, using two Pressler borer (length 100 and 300 mm and diameter 5.15 mm) (fig. 11) and we extracted at least two increment cores from each shrub. Only Pinus Mugo looking old were selected for sampling. All samples were prepared following standard dendrochronological procedures (Bräker, 2002), which consisted in air-drying, mounting and sanding of increment cores (with grit from 150, 240, 400 and 800). Tree rings were then counted and tree-ring widths were measured using a LINTAB-5 positioning table, connected to a Leica stereo-microscope and TSAP-Win Professional 4.64 software

During the lab analysis several samples were not dated, due to the impossibility of counting all the tree-rings. For this, only 20 shrubs were dated and their corresponding annual growing rate was calculated.

Fig. 11. Extracting cores from Pinus Mugo in Lovnitsa (a) and Popovo (b) rock glaciers.

As revealead in fig. 12 the shrubs installed on Popovo are much older compared with those from Lovnitsa. The average age of the Lovnitsa stand was 59 years, whereas on Lovnitsa the corresponding was 97.6 years. Thus, in site K1 only one sample was older than 100 years, whereas in case of Popovo, seven from a total of eleven are older than 100 years.

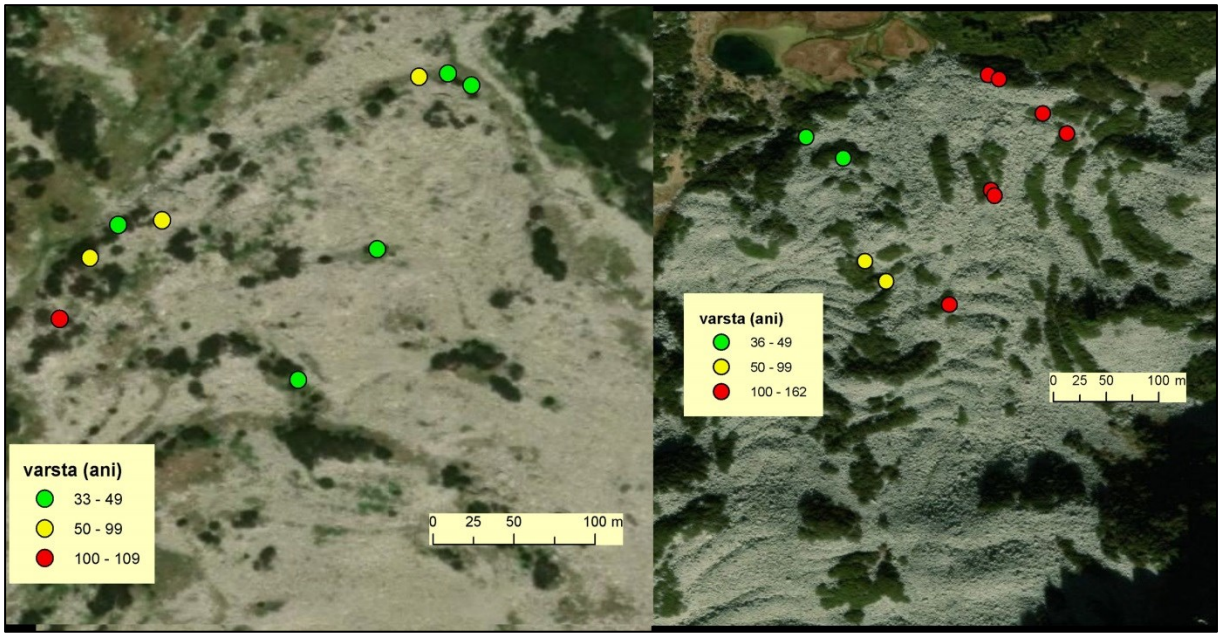

Fig. 12. Age structure of shrubs sampled on Lovnitsa (left) and Popovo (right) rock glaciers.

The mean multiannual growth rate was also considerably different between the two investigated stands (fig. 13). In case of Lovnitsa, the mean rate was 0.68 mm/year, whereas the corresponding for Popovo was only 0.39 mm/year. Only one shrub has a growth rate below 0.4 mm/year at Lovnitsa site, whereas in Popovo eight shrubs show a mean growth rate below this threshold. It is obvious that very young shrubs shows growth rates considerably higher than old shrubs.

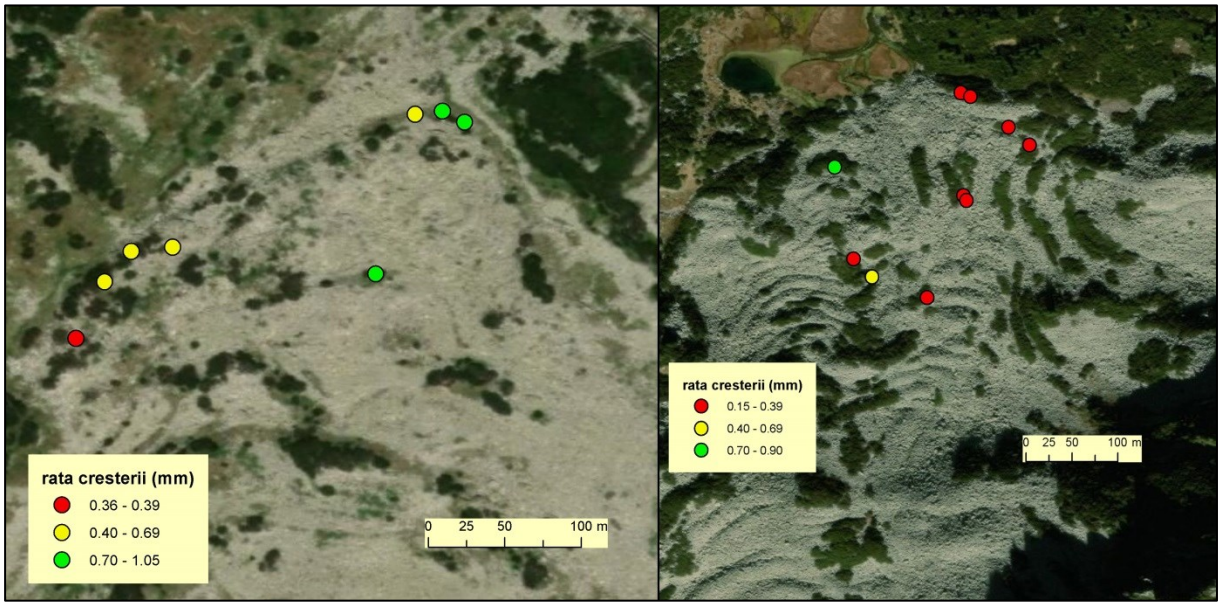

Fig. 13. Multiannual growth rates of shrubs sampled in Lovnitsa (left) and Popovo (right) rock glacier.

9. UAV photogrammetry and Structure from Motion for high resolution digital elevation model production and monitoring long term horizontal displacement of blocks.

The recent development of digital photogrammetry and computer vision algorithms (e.g. Structure from Motion), enabled the construction of high-resolution and high-accuracy digital elevation models at an affordable price compared to airborne LiDAR (light detection and ranging) technique (Cook, 2017). Using a cost-effective UAV Phantom 4 Pro equipped with a commercial digital camera we were capable to acquire high-density and high-accuracy 3D terrain point data for 15 sites.

The construction of high-resolution digital elevation models (DEM) (10-20 cm/pixel) will allow us to evaluate more carefully the differences in the surface elevation, and the role of topo-cimatic factors on GST regime. To geometrically correct the image locations during processing we used field ground control points with very accurate GPS systems (DGPS). The camera was setted to take pictrues every 3 seconds. All the acquired images were processed using Agisoft Photoscan Professional software, which uses photogrammetric algorithms to generate digital elevation models of the rock glaciers. The cloud points consisted on an initial cloud points counting tens of thousands of points. In addition, the drone aerial photographs allowed a more accurate delineation of the rock glaciers and of course served to better geomorphological mapping of the selected investigation sites. In the end we were able to produce an orthophoto for each investigated rock glacier. All the achieved digital elevation models had spatial resolution below 0.5 m/pixel, whereas the orthophotos had a resolution below 0.2 m/pixel.

The orthophotos and the digital elevation models of the rock glaciersare presented in figs. 14-26.

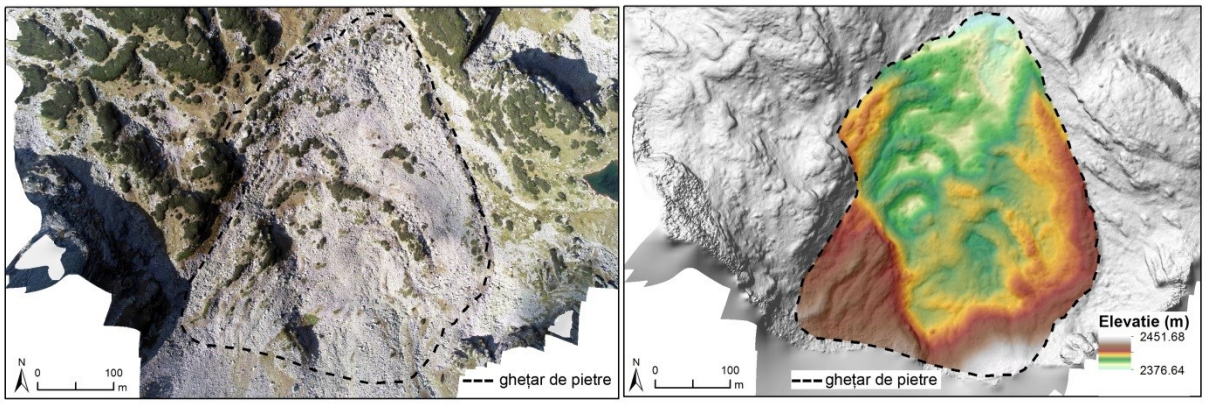

Fig. 14. Ortophoto and digital elevation model of the surface of K1.

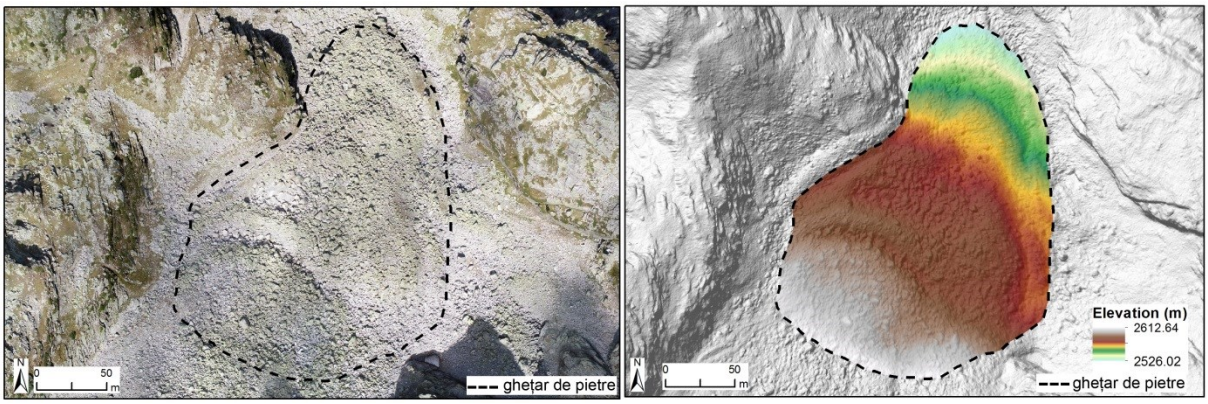

Fig. 15. Ortophoto and digital elevation model of the surface of K2.

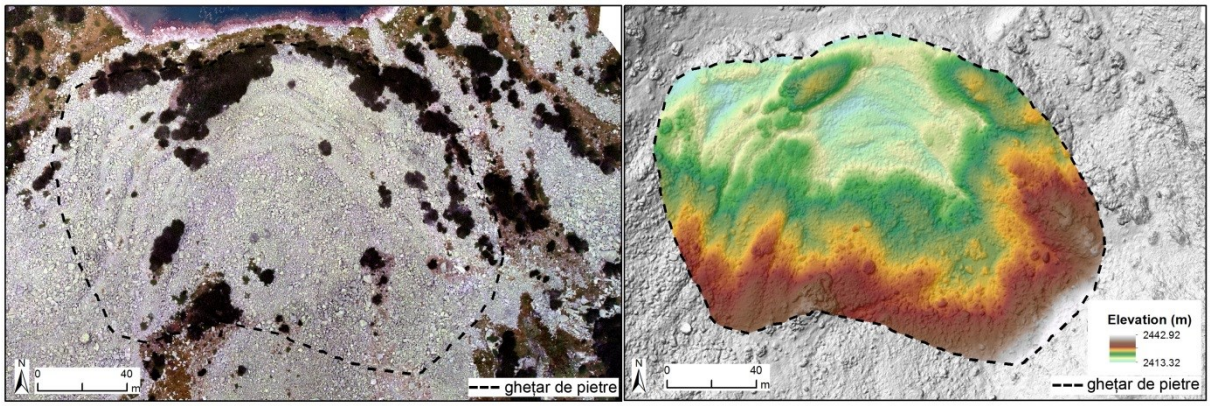

Fig. 16. Ortophoto and digital elevation model of the surface of M3.

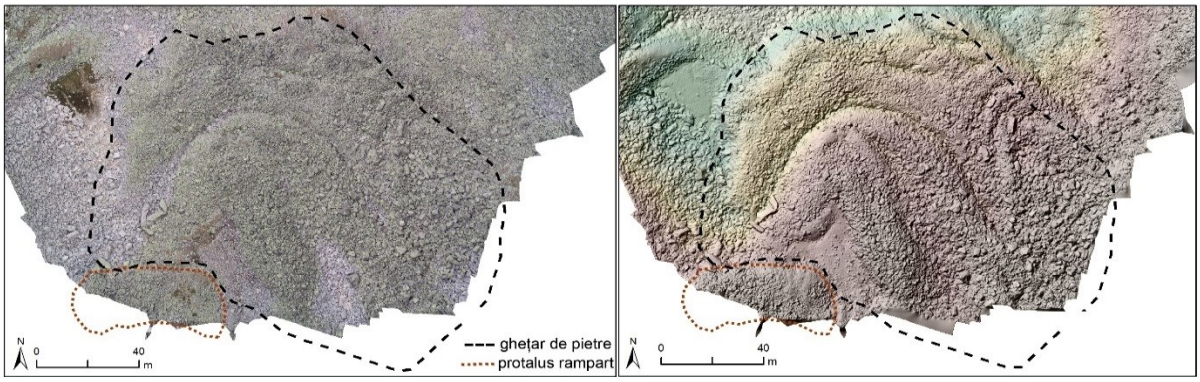

Fig. 17. Ortophoto and digital elevation model of the surface of M4.

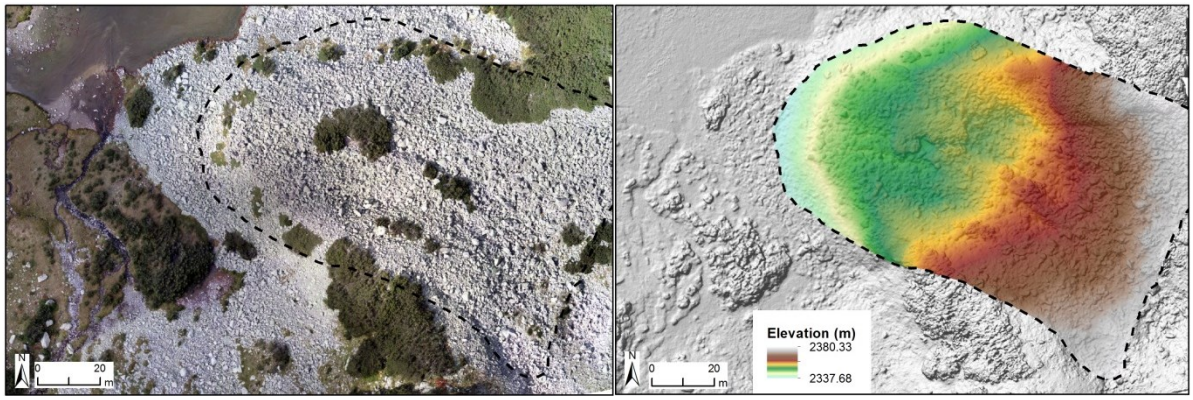

Fig. 18. Ortophoto and digital elevation model of the surface of P6.

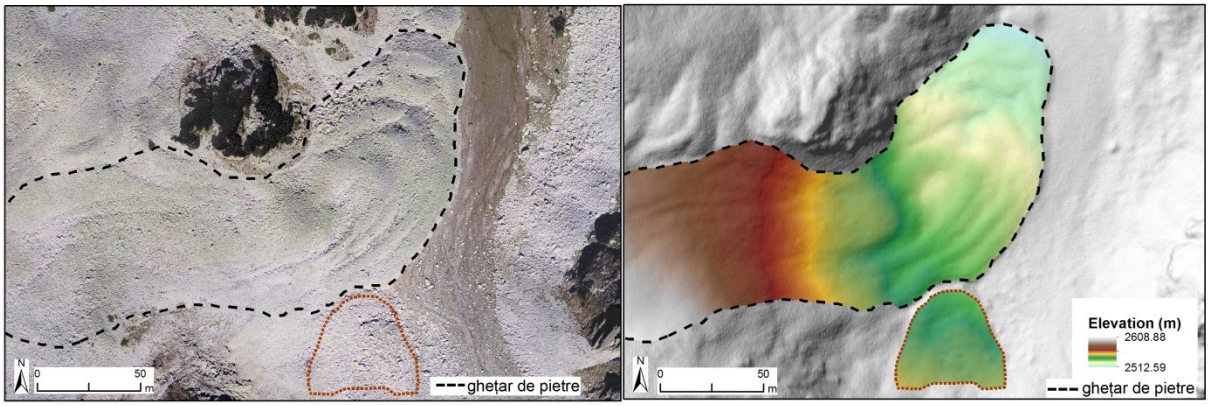

Fig. 19. Ortophoto and digital elevation model of the surface of P8.

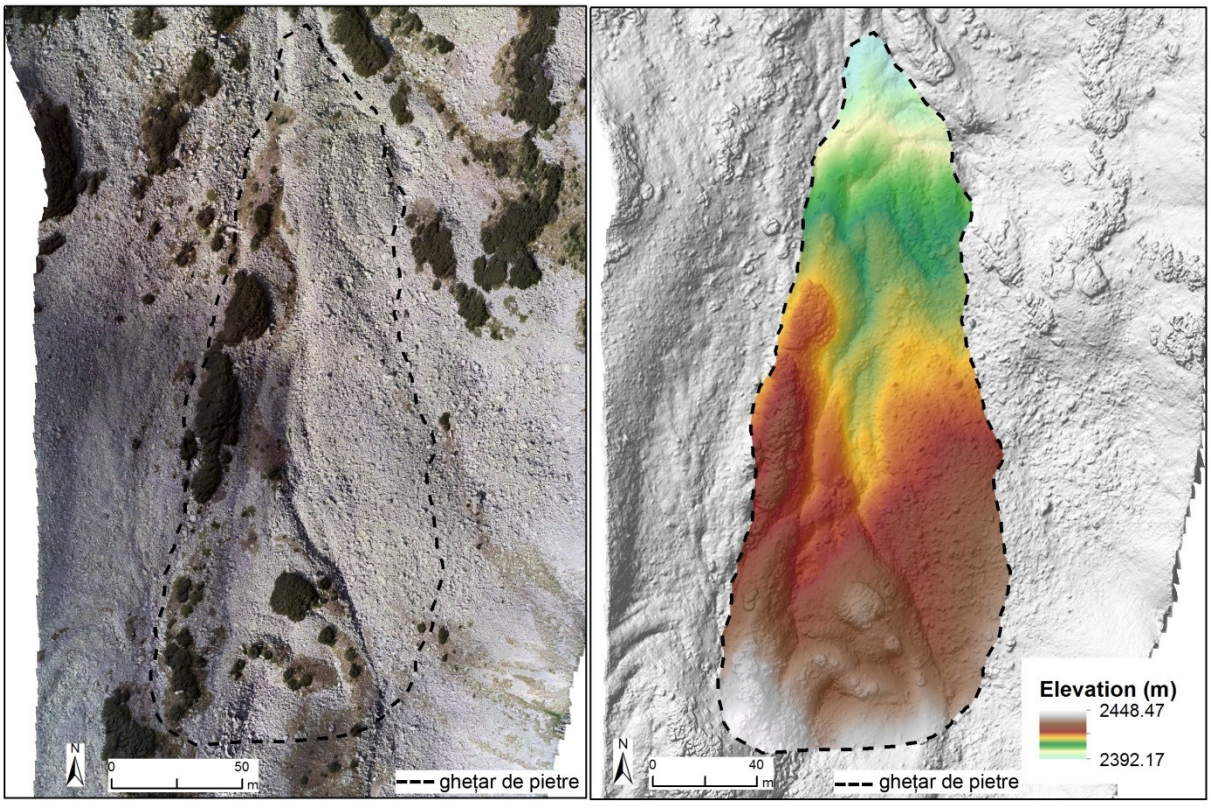

Fig. 20. Ortophoto and digital elevation model of the surface of P7.

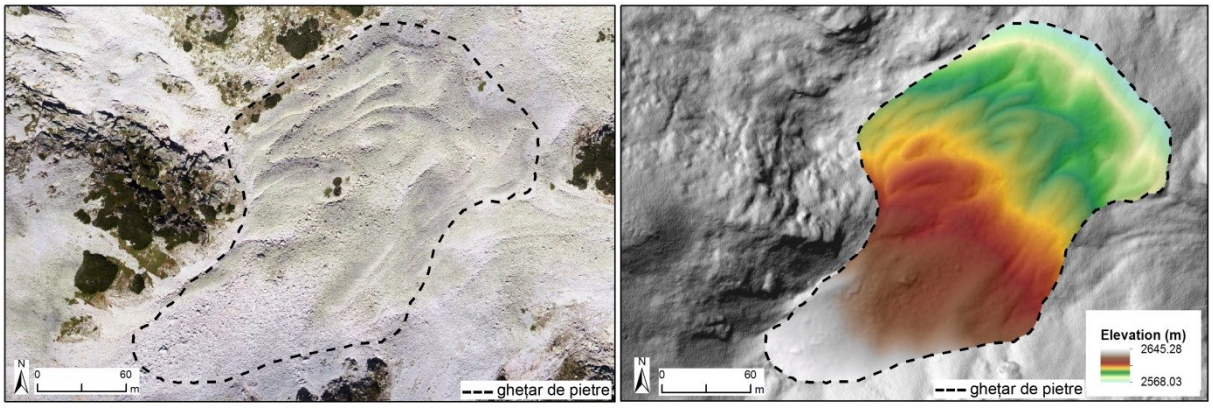

Fig. 21. Ortophoto and digital elevation model of the surface of P9.

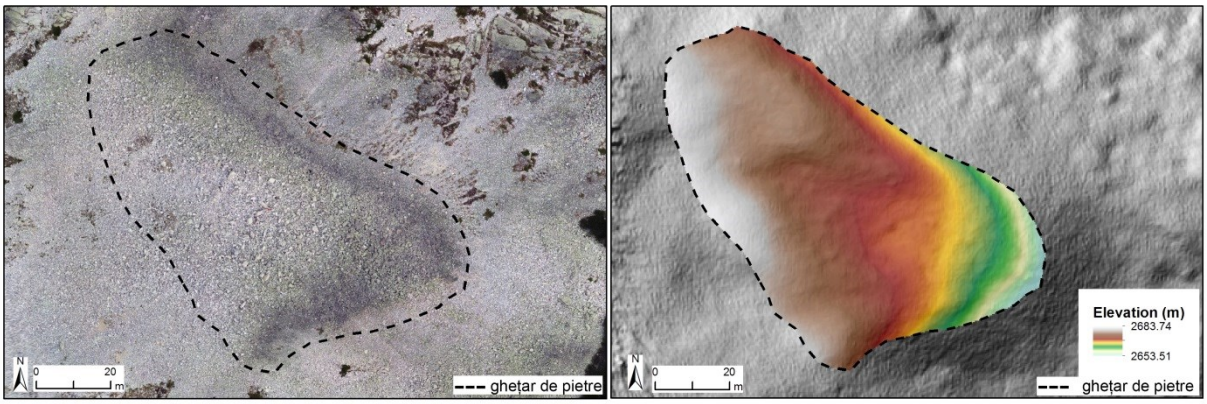

Fig. 22. Ortophoto and digital elevation model of the surface of P10.

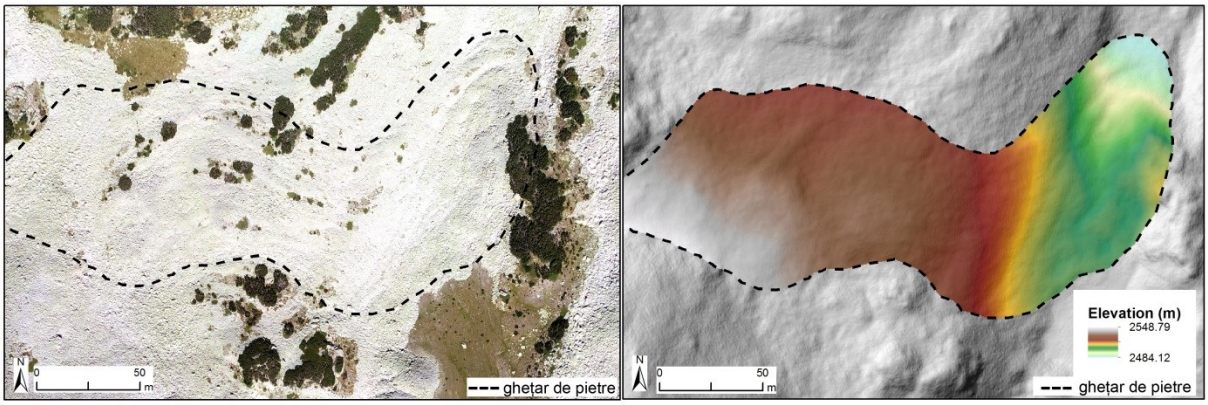

Fig. 23. Ortophoto and digital elevation model of the surface of P11.

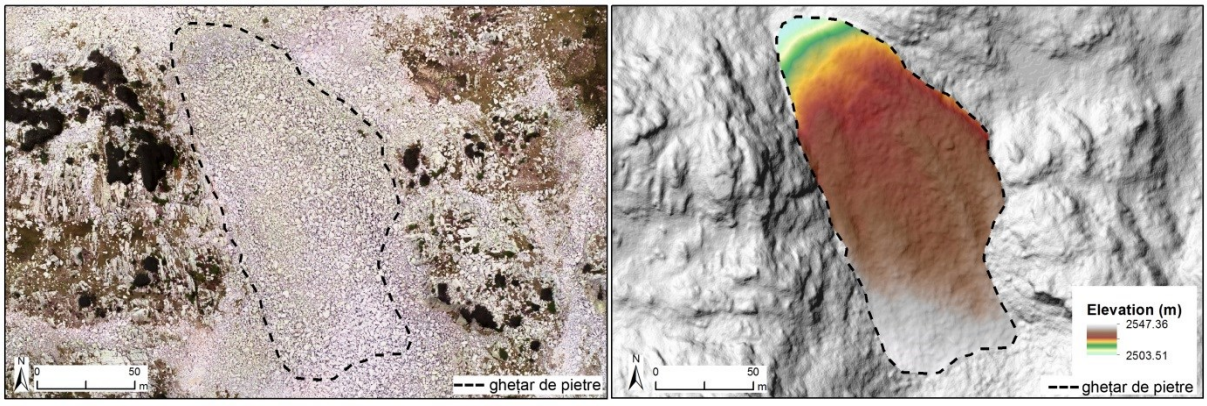

Fig. 24. Ortophoto and digital elevation model of the surface of B12.

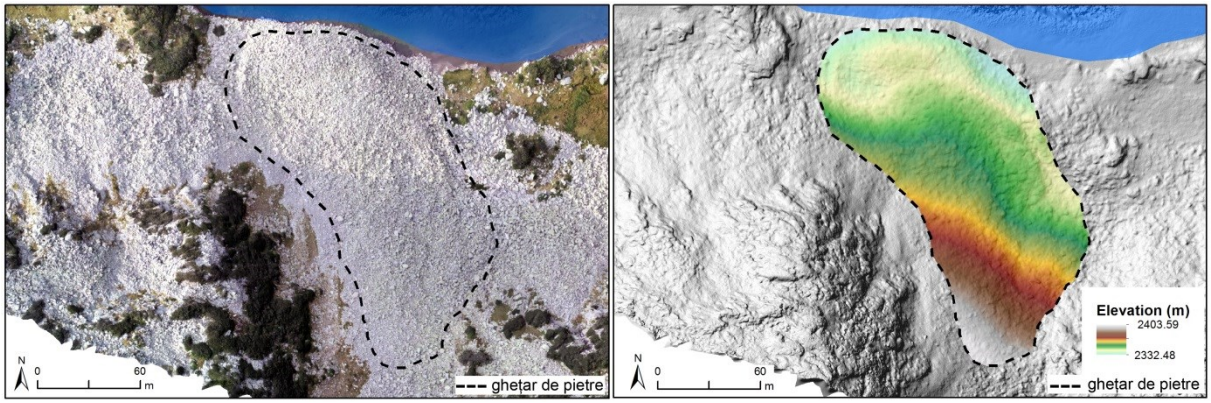

Fig. 25. Ortophoto and digital elevation model of the surface of B13.

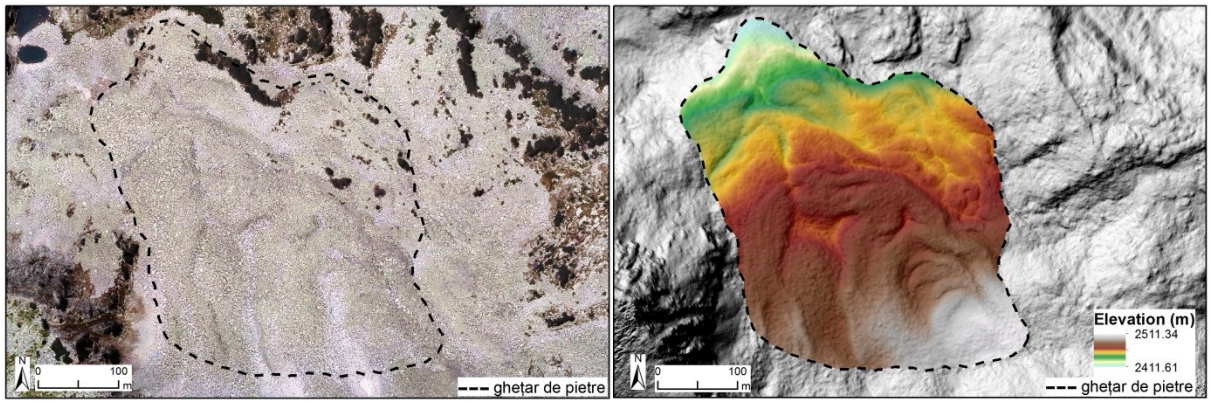

Fig. 26. Ortophoto and digital elevation model of the surface of B14.

Dissemination

For the dissemination of the most important information, the PERMBULG project web page was updated (https://permbulg.projects.uvt.ro/).

Conferences

- **Onaca, A.,** Ardelean, A., Ardelean, F., Gachev, E., Magori, B. Sîrbu, F., Ice thickness and internal structure of two small glaciers in the Pirin Mountains (Bulgaria) assessed by geophysical investigations, *INQUA 2019, Dublin, Ireland*, 25-31.07.2019;

- **Onaca, A.**, Voiculescu, M., Ardelean, F., Gachev, E., Urdea, P., Magori, B., Sîrbu, F., Thermal and morphological characteristics of rock glaciers in the Rila and Pirin Mountains, *Carpatho-Balkan-Dinaric Conference on Geomorphology, Szeged, Hungary*, 24-27.06.2019;

- **Onaca, A.,** Voiculescu, M., Magori, B., Sîrbu, F., Ardelean, F., Permafrost investigations in the highest mountains of Bulgaria and Romanian Carpathians (Romania), *Geobalcanica, Sofia, Bulgaria,* 13-14.06.2019;

- **Onaca, A.,** Voiculescu, M., Ardelean, F., Urdea, P., Gachev, E., Magori, B., Hegyi, A., Sîrbu, F., Băbănaș, M., 2019, Permafrost characteristics in marginal periglacial environment of Rila and Pirin Mountains, *35th Symposium on Geomorphology, Timișoara*, 23-26.05.2019;

- **Onaca, A.,** Ardelean, A., Magori, B., Voiculescu, M., Ardelean, F., Gachev, E., Sirbu, F., 2019, Permafrost investigations in the Rila and Pirin Mountains, Bulgaria, *EGU, Viena, Austria*, 7-12.04.2019;

Publications

- ***„Assessment of permafrost conditions in the highest mountains of the Balkan Peninsula,"*** (authors: Onaca A., Ardelean, F., Ardelean, A., Magori, B., Sîrbu, F., Voiculescu, M., Gachev, E.)**, Catena**, in press, https://doi.org/10.1016/j.catena.2019.104288.
- ***"Distribution and Characteristics of Rock Glaciers in the Balkan Peninsula"*** (autori: Magori, B., Urdea, P., Onaca A., Ardelean, F.), in evaluation.

Bibliography

Angelopoulos, M. C., Pollard, W. H. & Couture, N. J. 2013. The application of CCR and GPR to characterize ground ice conditions at Parsons Lake, Northwest Territories. *Cold Regions Science and Technology,* 85**,** 22-33.

Ardelean, A., Onaca, A., Urdea, P., Sărășan, A., 2017. Quantifying postglacial sediment storage and denudation rates in a small alpine catchment of the Făgăraș Mountains (Romania), *Science of the Total Environment*, 599-600, 1756-1767.

Bräker, O.U., 2002, *Measuring and data processing in tree-ring research — a methodological introduction.* Dendrochronologia 20, 203–216.

Cook, K., 2017. An evaluation of the effectiveness of low-cost UAVs and structure for motion for geomorphic change detection. *Geomorphology*, 195-208.

Gruber, S., Hoelzle, M., 2008. The cooling effect of coarse blocks revisited: amodeling study of a purely conductive mechanism. In: Kane, D.L., Hinkel, K. (Eds.), Ninth International Conference on Permafrost, Institute of Northern Engineering, University of Alaska, Fairbanks, pp. 557–561.

Hoelzle, M., Wegmann, M. & Krummenacher, B. 1999. Miniature temperature dataloggers for mapping and monitoring of permafrost in high mountain areas: first experience from the Swiss Alps. *Permafrost and Periglacial Processes,* 10**,** 113-124.

Ishikawa, M. 2003. Thermal regime at the snow–ground interface and their implications for permafrost investigation. *Geomorphology,* 52**,** 105–120.

Onaca, A., Ardelean, A. C., Urdea, P., Ardelean, F., Sîrbu, F., 2015, Detection of mountain permafrost by combining conventional geophysical methods and thermal monitoring in the Retezat Mountains, Romania, *Cold Regions Science and Technology*, 119, 111-123.

Onaca A., Ardelean, F., Ardelean, A., Magori, B., Sîrbu, F., Voiculescu, M., Gachev, E., in press. Assessment of permafrost conditions in the highest mountains of the Balkan Peninsula, *Catena*.

Otto, J.-C., Keuschnig, M., Götz, J., Marbach, M. & Schrott, L. 2012. Detection of mountain permafrost by combining highresolution surfaceandsubsurface information – an example from the Glatzbach catchment, Austrian Alps. *Geografiska Annaler: Series A, Physical Geography,* 94**,** 43-57.